Bioconjugate Chemistry

pubs.acs.org/bc Article

Interactions between Oligoethylene Glycol-Capped AuNPs and Attached Peptides Control Peptide Structure

Logan M. Wilder, Paul R. Handali, Lauren J. Webb,* and Richard M. Crooks*

Cite This: *Bioconjugate Chem.* 2020, 31, 2383−2391 Read Online

ACCESS | Metrics & More | Article Recommendations | Supporting Information

ABSTRACT: Peptide-functionalized nanoparticles (NPs) often rely on a well-defined peptide structure to function. Here, we report the attachment of model peptides to the ligand shell of AuNPs passivated with oligoethylene glycol (OEG). Specifically, peptides containing the repeating $(LLKK)_n$ motif plus either one or two reactive functional groups were covalently linked to OEG-capped, ∼5 nm AuNPs via the Cu^+-catalyzed azide−alkyne cycloaddition reaction. This work builds on a previous study from our group in which an $(LLKK)_n$ peptide having two reactive functional groups was considered. Peptide attachment was confirmed by FTIR spectroscopy. Amino acid analysis was used to determine that 3−4 peptides were immobilized per AuNP. Circular dichroism spectroscopy revealed a structural change from random coil in solution to α-helical upon attachment to OEG-capped AuNPs. The key result of this study is that the nature of the capping layer on the AuNP surface influences peptide structure to a significant degree. Other important findings resulting from this work are that the AuNP−peptide conjugates reported here are water soluble and that the long axis of the helical peptides is oriented tangent to the AuNP surface. The latter point is important for applications involving biorecognition.

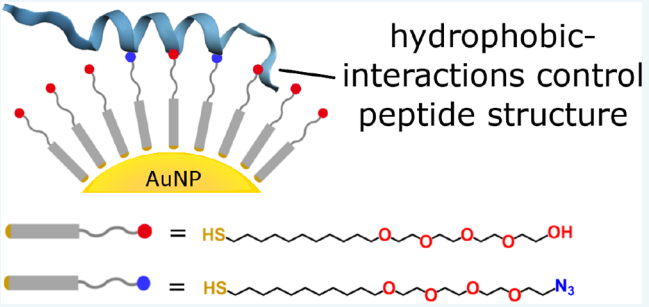

INTRODUCTION

Nanoparticle (NP)−peptide conjugate materials combine the unique properties of NPs with the biorecognition capabilities of peptides.[1−3] For example, surface-confined peptides can recognize and bind biomolecules or direct NPs to precise locations within biomaterials. Specifically, NP−peptide conjugates have been used to deliver NPs to the interior of cells,[4] selectively stain tissue,[3] and enable advanced chemical sensing schemes.[5] In some important cases recognition depends on the secondary structure of the peptide. For example, β-sheet-structured peptides on NPs bind to β-amyloid fibrils more strongly than unstructured peptides.[6] In addition, α-helical peptide-functionalized AuNPs have been found to mimic protein−protein interactions by binding a target protein.[7] For applications such as these, conformational stability of the peptide is crucial, but there are numerous examples demonstrating that this can be difficult to control.[8−10]

In addition to their secondary structure, peptide orientation relative to NPs (e.g., perpendicular vs tangent to the NP surface) is also important for molecular recognition. For helical peptides, recognition interactions between the peptide and other biomolecules generally occur parallel to the helical axis.[11] Several reports describe NP−peptide conjugates in which the conformation of the peptide was α-helical but the helix was oriented perpendicular to the NP.[9,12−14] Due to the steric hindrance between the peptide chains, however, this orientation can result in the bulk of the peptide side chain being shielded from solution. Other reports describe NP−peptide conjugates in which helical peptides are electrostatically bound to NPs in parallel orientations. These conjugates also have limitations due to weak and pH-dependent electrostatic interactions between the NPs and the peptides.[15,16]

We recently reported a general strategy for synthesizing water-soluble, AuNP−peptide conjugates in which the peptides are present primarily in α-helical conformations and are oriented parallel to the NP surface.[17] This configuration is shown in Scheme 1, where a ∼5 nm AuNP stabilized with alkylthiol/oligoethylene glycol (OEG) ligands is covalently modified with a leucine/lysine $(LLKK)_n$ peptide which undergoes a random coil to an α-helical structure change when it transitions from solution to the surface of the AuNP. We hypothesized that nonpolar regions of the peptide preferentially associated with the OEG layer and that this resulted in the aforementioned conformational change. In this case the peptide was attached to the OEG surface at two sites

Received: August 8, 2020
Revised: September 8, 2020
Published: September 24, 2020

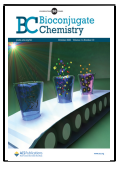

https://dx.doi.org/10.1021/acs.bioconjchem.0c00447
Bioconjugate Chem. 2020, 31, 2383−2391

Scheme 1

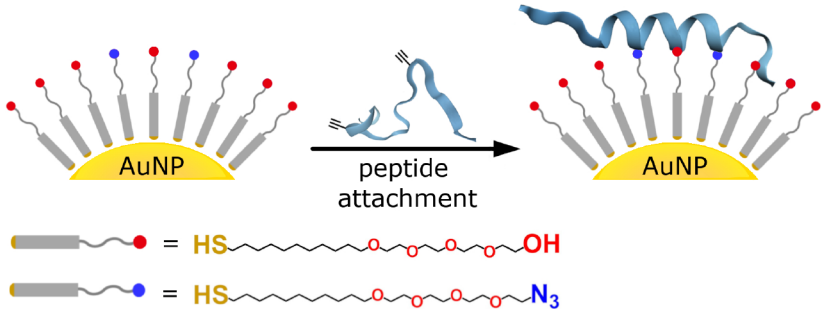

however, and thus, the structural change could also have been driven by a helix-stapling mechanism[18] or a combination of factors. Understanding the forces that control peptide structure on OEG-modified AuNPs was a principal reason for undertaking the present study.

We used a ligand with the ethylene glycol (EG) motif for our earlier study because OEG and polyethylene glycol (PEG) are widely used for maintaining NP solubility in aqueous solutions and for preventing nonspecific adsorption of proteins.[4,19−21] Specifically, NPs stabilized with OEG/PEG ligands are known to remain colloidally stable at high ionic strengths and in concentrated protein solutions, such as in biological milieu. In addition, these ligands are often used for attaching biomolecules to NPs to prevent destabilizing interactions between the NPs and the biomolecules to which they are conjugated.[21−25]

Despite the wide technological use of the EG motif, there have only been a few reports describing the nature of the interactions between peptides and OEG/PEG-functionalized NPs. For example, a study of amyloid-beta peptide (Aβ) and PEG-functionalized NPs revealed that the peptide interacted more strongly with the PEG-modified NPs than with free PEG chains, suggesting a peptide binding mechanism involving multiple PEG chains on the NP.[26] Another study found that cofunctionalization of NPs with EG and peptides sometimes enhanced the colloidal stability of NPs to a greater extent than just peptides.[27]

In the present article, we report the synthesis and characterization of alkylthiol/OEG-capped, ∼5 nm AuNPs functionalized with $(LLKK)_n$ peptides. Two versions of a repeat $(LLKK)_n$ sequence peptide were investigated: one version in which the peptide displayed a single functional group for covalent attachment to the AuNPs and another in which the peptide displayed two possible attachment points. The results obtained using the $(LLKK)_n$ peptides having two attachment sites to the AuNPs were consistent with findings in our previous work.[17] As briefly mentioned earlier, Scheme 1 is an illustration showing the conjugation strategy for preparing these materials. Fourier transform infrared (FTIR) spectroscopy, circular dichroism (CD) spectroscopy, and amino acid analysis (AAA) confirmed the presence of 3−4 covalently bound peptides per AuNP. They also indicated the peptides are mostly in a random coil configuration when free in solution but adopt a helical conformation on the surface of the AuNPs. The results further show that the change in structure is driven by hydrophobic interactions between the peptides and the capping OEG layer of the AuNPs. Taken together, these results provide a detailed molecular-level understanding of the overall structure of the entire AuNP−peptide construct, making this an ideal model for future studies of the interaction between NP−peptide conjugates and proteins or other biomolecules.

RESULTS AND DISCUSSION

Synthesis and Modification of AuNPs. The NPs used in this work (AuNP-OEG4-N_3/OH) consisted of 4.6 ± 1.2 nm Au cores (Figure S1) capped with HS-$(CH_2)_{11}$-O-$(CH_2$-CH_2-$O)_3$-CH_2-CH_2-X (hereafter referred to as HS-C11-OEG4-X), where X = OH or N_3.[17] FTIR spectroscopy (Figures S2 and S3 and the associated discussion in the Supporting Information) indicated that ∼16% of the molecules in the ligand shell were terminated in $-N_3$ and the balance in −OH. The −OH terminal groups ensure the aqueous solubility of AuNP-OEG4-N_3/OH, while the $-N_3$ groups function as attachment points for the alkyne-functionalized peptides. AuNP-OEG4-N_3/OH is soluble in water, as demonstrated by UV−vis spectroscopy (Figure S4).[28]

The diameter of AuNP-OEG4-N_3/OH, accounting for the contribution of both the Au core and the fully extended ligands, is 10.6 ± 1.2 nm (see the Supporting Information for a discussion of this calculation).[29] The choice of this size was determined by two factors. First, as the size decreases, surface curvature increases. If the surface curvature is too severe, it is possible that the 20-mer peptide would not form a helix due to destabilizing strain effects. Scheme 2 displays a scale model of AuNP-OEG4-N_3/OH having four 20-mer helical peptides attached. Here, the curvature of the 10.6 nm sphere (AuNP core + HS-C11-OEG4-N_3/OH shell) is small compared with the long axis of the 20-mer peptide helix.

Scheme 2

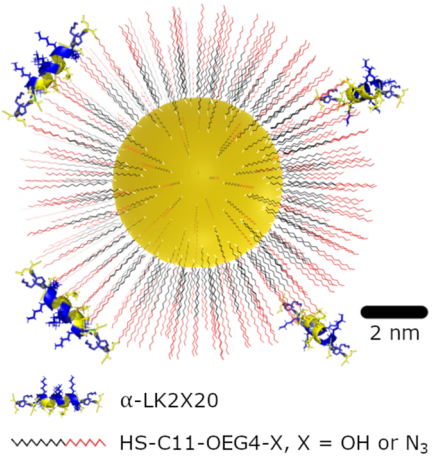

https://dx.doi.org/10.1021/acs.bioconjchem.0c00447
Bioconjugate Chem. 2020, 31, 2383−2391

The second reason for the choice of NP size has to do with the optical absorbance of metal NPs in the 190−250 nm range. According to Mie theory, the absorbance of spherical NPs much smaller than the wavelength of light increases as a function of the volume of the NP.[30] Hence, larger AuNPs would lead to opaque solutions and thus preclude the use of the information-rich 190−250 nm region in CD spectroscopy that is essential for characterizing the peptide structure. Taking this into consideration, ∼5 nm AuNPs provided a good balance between the need to minimize the strain of the peptide structure and still making CD spectroscopy available for characterization.

FTIR Analysis of Peptide Attachment to AuNPs. The peptides used in the present study were LKKLXKKLLKKLLKKGLKKL (α-LK1X20) and LKKLXKKLLKKLLKKXLKKL (α-LK2X20), where X = propargylglycine. Both α-LK1X20 and α-LK2X20 contain the $(LLKK)_n$ repeat unit, an α-helix-forming peptide sequence which has been used previously to investigate the structure of peptides at interfaces.[31−37] The conformational behavior of $(LLKK)_n$ peptides will be discussed in detail below.

Both α-LK1X20 and α-LK2X20 contain the noncanonical amino acid propargylglycine (X in the sequences). Propargylglycine displays an alkyne-terminated R group, which allows attachment of α-LK1X20 or α-LK2X20 to AuNP-OEG4-N_3/OH using the Cu^+-catalyzed azide−alkyne cycloaddition (CuAAC) reaction.[38] Importantly, the CuAAC reaction is bioorthogonal, which means that neither functional group required for the reaction readily reacts with functional groups typically found in biomolecules. This is an important property of reactions involving peptides.

To attach peptides to AuNPs, AuNP-OEG4-N_3/OH and α-LK1X20 or α-LK2X20 were incubated together in the presence of Cu^+ for 18 h, and then the AuNP solutions were filtered using molecular weight cutoff filters to separate small molecule reactants and unattached peptides from the AuNPs. The FTIR spectrum of AuNP-OEG4-N_3/OH-α-LK1X20 is shown in Figure 1 (red spectrum). The amide I and II peaks at 1656 and 1544 cm^{-1}, respectively, demonstrate that in the presence of Cu^+ α-LK1X20 attaches to the AuNPs. Note that the spectrum of the peptide alone (green) exhibits these same amide peaks at nearly the same locations: 1658 and 1544 cm^{-1}. The spectrum of AuNP-OEG4-N_3/OH-α-LK1X20 (red) also contained the azide N═N stretch at 2101 cm^{-1}, indicating that some of the azide groups in the AuNP-confined monolayer do not react.

We carried out a negative control experiment to confirm that the peptides are covalently linked to the AuNPs. AuNP-OEG4-N_3/OH was incubated with α-LK1X20 but in the absence of the Cu^+ catalyst required for the CuAAC reaction. Next, unreacted peptide was removed from the solution by filtration. Finally, the FTIR spectrum of the α-LK1X20-exposed AuNP-OEG4-N_3/OH was obtained (Figure 1, black). There are two important outcomes of this experiment. First, the control spectrum does not exhibit peaks in the amide region, which means that the peptides do not physisorb to AuNP-OEG4-N_3/OH. Second, the height of the azide peak at 2101 cm^{-1} is slightly higher than that of the corresponding peak in the red spectrum, indicating that when the Cu^+ catalyst is present in solution a small percentage of the azide groups reacts. Taken together, these two results confirm covalent attachment of α-LK1X20 to AuNP-OEG4-N_3/OH only in the presence of the Cu^+ catalyst through the cycloaddition reaction.

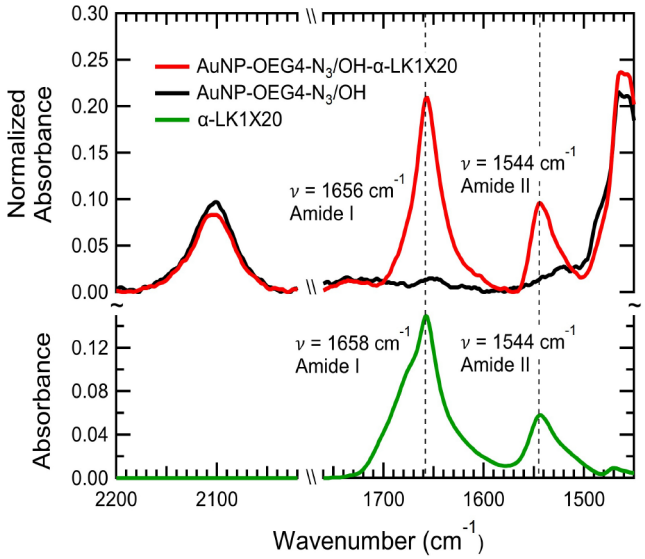

Figure 1. FTIR spectra of the α-LK1X20 peptide, AuNP−peptide conjugate, and control AuNPs: (green) α-LK1X20; (red) AuNP-OEG4-N_3/OH which was incubated with α-LK1X20 in the presence of the Cu^+ attachment catalyst and then separated from unreacted peptide by filtration; (black) AuNP-OEG4-N_3/OH which was incubated with α-LK1X20 but in the absence of the attachment catalyst and then separated from unreacted peptide by filtration. All FTIR spectra were collected by drop casting and drying the reagent solution onto a CaF_2 disk and then collecting and averaging 500 scans. Procedure for processing the spectra is provided in the Materials and Methods.

The same set of conditions used to obtain the spectra shown in Figure 1 were also used for the other peptide in this study, α-LK2X20. The results of this study, which are very similar to those reported in our previous work,[17] are shown in Figure S5. The FTIR data reveal that α-LK2X20 attachment to AuNP-OEG4-N_3/OH is similar to the attachment of α-LK1X20. Specifically, α-LK2X20 covalently attaches to AuNP-OEG4-N_3/OH, the majority of azide functional groups are still present on AuNP-OEG4-N_3/OH after attachment, and unattached α-LK2X20 was removed from solution by the filtration procedure described earlier.

It is possible to estimate the average number of peptides covalently linked to each AuNP using eq 1 and the results in Figures 1 and S5.

$$\frac{A \times f}{B} = n \tag{1}$$

Here, A represents the number of azide functional groups per AuNP, B is the number of alkyne functional groups per peptide, f is the fraction of azide functional groups which reacted when the Cu^+ catalyst was present (e.g., the fractional decrease in the height of the azide peak at 2101 cm^{-1} in the red spectrum as compared with the corresponding peak in the black spectrum in Figure 1), and n is the estimated number of peptides per AuNP.

To determine A, the total number of thiolated ligands per AuNP was calculated by multiplying the average geometric surface area of the Au core of AuNP-OEG4-N_3/OH by the estimated number of ligands per nm^2.[39] Next, the total number of −OH plus $-N_3$-terminated ligands was multiplied by the fraction of N_3-terminated ligands (∼0.16, as discussed in the previous section).

https://dx.doi.org/10.1021/acs.bioconjchem.0c00447
Bioconjugate Chem. 2020, 31, 2383−2391

The value of B comes from the known sequences of the two synthetic peptides. For α-LK2X20, an assumption in eq 1 is that both alkyne groups in every peptide react with the organic monolayer. The value of f is determined by comparing the heights of the azide peaks at 2101 cm^{-1} in the presence and absence of covalently linked peptides (Figure 1, red and black spectra). Specifically, the fraction of azide groups that react with alkyne functional groups of the peptides directly correlates to f.

To estimate the number of peptides per AuNP, we carried out three independent syntheses and then obtained FTIR data like that shown in Figure 1. The azide IR absorbance values of the peptide-functionalized AuNPs and control AuNPs, as well as details of the calculation of the number of peptides per AuNP are provided in the Supporting Information. The results of this spectroscopic analysis indicate that AuNP-OEG4-N_3/OH-α-LK1X20 and AuNP-OEG4-N_3/OH-α-LK2X20 display 2.3 ± 0.6 and 2.6 ± 0.7 peptides per AuNP, respectively. The uncertainties reported in these measurements represent variability in AuNP size (4.6 ± 1.2 nm), variability in the height of the azide absorbance peaks at 2101 cm^{-1} for the three independent FTIR spectra, and the rather small differences between the peak heights of the samples with covalently attached peptide compared with those with no attached peptide.

Due to the significant uncertainty in the number of peptides per AuNP, we view the results of this analysis as qualitative. As we will discuss later, more reliable data are required to estimate the degree of helicity of the peptides. AAA is the gold standard method for determining the number of peptides of fixed composition in a sample,[40] and therefore, we carried out AAA of the AuNP−peptide conjugate samples.

Amino Acid Analysis (AAA) of Peptide Attachment to AuNPs. To measure the peptide loading of the AuNP−peptide conjugates, we carried out AAA of the AuNP−peptide conjugates.[40] For the AAA procedure used here, the AuNP−peptide conjugate solution was first dried under vacuum and then the samples were subjected to a high-temperature HCl vapor to hydrolyze the peptide portion of the conjugates. Next, the resulting amino acids were derivatized with o-phthalaldehyde, and then they were immediately quantified by HPLC with fluorescence detection. Extensive control experiments were conducted to ensure that the AAA results were not significantly affected by the presence of AuNPs. These are described in the Supporting Information (Figure S6 and associated discussion). The AAA indicated that the number of peptides per AuNP for AuNP-OEG4-N_3/OH-α-LK1X20 and AuNP-OEG4-N_3/OH-α-LK2X20 was 3.9 ± 0.1 and 3.5 ± 0.2, respectively. These quantitative values determined by AAA can be compared to the rather qualitative values determined by FTIR: 2.3 ± 0.6 and 2.6 ± 0.7, respectively.

We also used AAA to confirm that the peptides are only present on AuNP-OEG4-N_3/OH when linked covalently (i.e., the absence of nonspecific adsorption). The samples for this experiment were generated by first incubating AuNP-OEG4-N_3/OH with α-LK2X20 (but without the Cu^+ attachment catalyst) followed by filtration to remove unreacted peptide. AAA indicated no detectable level of peptide present in the retained AuNPs. This result confirms the FTIR finding that the peptide is neither covalently bound nor physisorbed to AuNP-OEG4-N_3/OH in the absence of the Cu^+ catalyst and after the filtration procedure.

Scheme 2 is a scale model of a AuNP−peptide conjugate that is consistent with the transmission electron microscopy (TEM), FTIR, and AAA results discussed thus far. The low surface density of peptide decreases the likelihood of peptide−peptide interactions compared with NPs displaying high surface coverages. This is useful as peptide−peptide interactions can potentially change the peptide structure and thereby alter the physical characteristics of the system.[9] The relative isolation of the peptides in the AuNP−peptide conjugates presented here is important because each peptide interacts only with the OEG4 surface and the solvent. This simplifies modeling and analysis of NP−peptide conjugates. The low peptide density also allows subsequent surface chemistry to be conducted on the unreacted and solvent-exposed HS-C11-OEG4-N_3/OH ligands. This may be useful for potential applications, such as attachment of additional biomolecules to the AuNP−peptide conjugates or immobilization of the AuNP−peptide conjugates on a surface.

Determination of Peptide Secondary Structure for AuNP−Peptide Conjugates. Peptides composed of repeating sequences of L and K amino acids were first shown to be versatile models for studying peptide behavior at interfaces by DeGrado and Lear.[41] A prominent example is the family of peptides with the $(LLKK)_n$ motif, which attains an α-helical structure at nonpolar−polar molecular interfaces. This type of interface includes, for example, the one that forms between water and a self-assembled monolayer displaying a hydrophobic headgroup.[42] This conformational transition to an α-helix occurs because the hydrophobic L and hydrophilic K residues partition on opposite sides of the longitudinal axis of the peptide when the peptide is helical. Accordingly, orthogonal interactions between L/K and the hydrophobic/hydrophilic phases, respectively, stabilize the α-helical structure.[31,37] This property of peptides containing the $(LLKK)_n$ motif has been used in previous studies for designing antimicrobial agents[43,44] and for templating well-defined nanostructures.[35] As mentioned previously, the two peptides used in the present study, α-LK1X20 and α-LK2X20, contain the α-helix-forming $(LLKK)_n$ motif. These peptides were chosen for the current work because of the effect of the $(LLKK)_n$ repeat unit on secondary structure.

Our prior work demonstrated that α-LK2X20 attains an α-helical structure when situated between water and a nonpolar self-assembled monolayer of alkylthiols on a planar Au substrate[45] or when attached to OEG-capped AuNPs dispersed in water.[17] In the current study, CD spectroscopy was used to quantitatively determine the constituent secondary structure components of α-LK1X20 and α-LK2X20 attached to AuNP-OEG4-N_3/OH. Structural characterization of the NP−peptide conjugates provided insight into the interaction between the peptides and the OEG monolayer.

CD spectroscopy is often used to evaluate the secondary structure of proteins in solution, but it has also been used to study surface-attached peptides.[7,15,42,46] Accordingly, we used CD to evaluate the peptides in the present study. As a control, the CD spectrum of AuNP-OEG4-N_3/OH with no attached peptides was obtained to ensure that it did not exhibit significant features over the wavelength range studied. As shown in Figure S7, this spectrum is featureless, and thus any CD features in the AuNP−peptide conjugates must arise from the surface-bound peptides.

Figure 2 presents the CD spectroscopy of unconjugated peptides and NP−peptide conjugates. The spectra of α-

https://dx.doi.org/10.1021/acs.bioconjchem.0c00447
Bioconjugate Chem. 2020, 31, 2383−2391

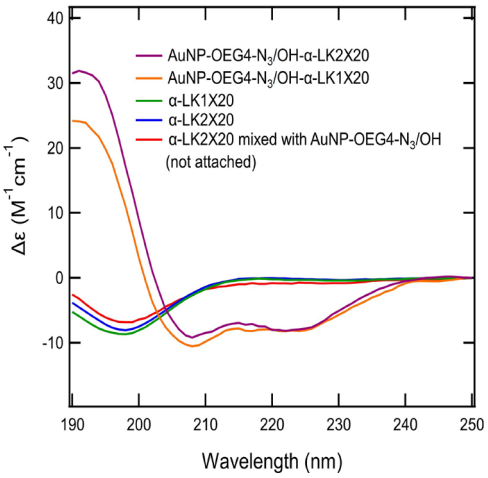

Figure 2. CD spectra of peptides and AuNP−peptide conjugates: (green) 30.0 μM α-LK1X20; (blue) 30.0 μM α-LK2X20; (orange) 1.24 μM AuNP-OEG4-N_3/OH-α-LK1X20; (purple) 1.21 μM AuNP-OEG4-N_3/OH-α-LK2X20; (red) 3.00 μM α-LK2X20 in the presence of (but not attached to) 1.04 μM AuNP-OEG4-N_3/OH. All spectra were recorded in deionized water using a 1.00 mm cuvette. Procedures used for obtaining and processing the spectra are provided in the Materials and Methods. Peptide-only spectra (green and blue) were generated by averaging 6 scans. AuNP−peptide conjugate spectra (purple and orange) were generated by averaging 500 scans. CD spectrum of α-LK2X20 in the presence of (but not attached to) AuNP-OEG4-N_3/OH (red) was also generated by averaging 500 scans.

LK1X20 and α-LK2X20 will be discussed first. The CD spectra of both α-LK1X20 and α-LK2X20 (green and blue spectra, respectively, in Figure 2) were obtained using solutions of unconjugated peptide in deionized (DI) water. All CD spectra, including the spectra of α-LK1X20 and α-LK2X20, were background corrected following a two-step procedure discussed in detail in the Supporting Information. Briefly, the spectrum of a solvent blank was subtracted from the sample spectrum. The resulting spectrum was further corrected by subtracting the signal at 250 nm from the remainder of the spectrum. This latter step ensures a zero baseline in a nonabsorbing part of the spectrum. A representative, unprocessed CD spectrum of AuNP-OEG4-N_3/OH-α-LK1X20, which is not blank subtracted, and the corresponding DI water solvent blank spectrum are shown in Figure S8.

The spectra of both α-LK1X20 and α-LK2X20 in aqueous solution exhibit a single minimum at 198 nm. This spectroscopic feature is characteristic of a primarily random-coil structure.[47,48] More quantitative information can be obtained by deconvoluting these spectra into fractional secondary structure elements. This was accomplished using the online deconvolution server BeStSel.[49,50] Table 1 shows that this analysis indicates the peptides are indeed present primarily in a random-coil configuration in DI water.

A control experiment was also carried out in which α-LK2X20 was added to a solution containing AuNP-OEG4-N_3/OH, but in this case the peptide and AuNPs were not covalently attached. The CD results (Table 1 and Figure 2, red spectrum) showed that the peptide in this case is also primarily present in a random-coil configuration. This result indicates that either α-LK2X20 did not adsorb strongly to AuNP-OEG4-N_3/OH or, if it did, adsorption did not cause a major structural change in the peptide in the absence of covalent linking.

In contrast to unconjugated α-LK1X20 and α-LK2X20, the CD spectra of α-LK1X20 and α-LK2X20 following covalent linking to AuNPs (orange and purple spectra in Figure 2) display double-trough character with minima at 208 and 222 nm. This shape is characteristic of an α-helical structure.[51] As shown in Table 1, structural deconvolution of AuNP-conjugated α-LK1X20 and AuNP-conjugated α-LK2X20 indicates 50% and 46% helical character, respectively.

As discussed earlier, $(LLKK)_n$ peptides characteristically attain helical structure at nonpolar/polar molecular interfaces due to favorable interactions between L with the nonpolar phase and K with the polar phase.[31−37] We observed this previously for α-LK2X20 conjugated to OEG-capped AuNPs.[17] However, because α-LK2X20 may bind to the AuNP in two positions, the driving force for the helical structural change could be hydrophobic interactions between the peptide and the OEG layer, a helix stapling effect,[18] or some combination of these two factors. In contrast, α-LK1X20 is not capable of "stapling" to AuNP-OEG4-N_3/OH at multiple points, and therefore, the driving force for helix formation is unambiguously hydrophobic interactions between the leucine side chains and the OEG layer of AuNP-OEG4-N_3/OH. This is a key result because it demonstrates that the design of bio/abiointerfaces must take into account both noncovalent and covalent (e.g., bioconjugation) interactions.

This latter point is particularly important because hydrophobic interactions between a substrate and peptides or proteins typically result in loss of defined secondary structure of the biomolecule followed by aggregation and/or loss of function.[52] In the particular case of the $(LLKK)_n$ peptides used in this work, this situation is reversed as it is clear that hydrophobic interactions are responsible for attainment of the α-helix structure upon attachment to the OEG layer. This point further suggests that the helical axes of the peptides are oriented parallel to the AuNP surface as illustrated in Scheme 2.

Peptides having an α-helical structure are notable recognition elements in protein−protein and protein−DNA interactions.[53−56] Accordingly, the AuNP−peptide conjugates

Table 1. Percentage Conformation of Unconjugated Peptides and AuNP-Conjugated Peptides (as predicted by BeStSel)[a]

structure type[b]	α-LK1X20	α-LK2X20	α-LK2X20 plus AuNP-OEG4-N_3/OH (not attached)	AuNP-OEG4-N_3/OH-α-LK1X20	AuNP-OEG4-N_3/OH-α-LK2X20
helix	0%	0%	2%	50%	46%
strand	35%	37%	31%	6%	20%
turn	16%	14%	18%	13%	13%
others	49%	50%	48%	31%	21%

[a]From left to right, 30.0 μM α-LK1X20, 30.0 μM α-LK2X20, 3.00 μM α-LK2X20 in the presence of (but not attached to) 1.04 μM AuNP-OEG4-N_3/OH, 1.24 μM AuNP-OEG4-N_3/OH-α-LK1X20, and 1.21 μM AuNP-OEG4-N_3/OH-α-LK2X20. All data were obtained using DI water as the solvent. [b]The normalized root-mean-square deviation (NRMSD) was below 0.05 in all cases.

https://dx.doi.org/10.1021/acs.bioconjchem.0c00447
Bioconjugate Chem. 2020, 31, 2383−2391

reported here should be useful motifs for designing NPs displaying peptides in an α-helical conformation that function as biorecognition elements. Importantly, the synthetic approach we described leads to peptides having their longitudinal axis tangent to the AuNP substrate. In turn, this results in a solution-facing surface of amino acids tailored to enhance interactions with, for example, a target protein. Work toward this goal is ongoing.

SUMMARY AND CONCLUSIONS

We examined two versions of a AuNP−peptide conjugate model system exhibiting $(LLKK)_n$ peptides to better understand and control interactions between the peptides and the OEG-capped AuNP substrates. The key finding is that covalent attachment of the two peptides we examined to azide-functionalized, OEG-capped AuNPs leads to a change in peptide structure from primarily random coil to primarily α-helix. CD analysis indicates that both peptides exhibit similar magnitudes of helix, strand, turn, and random coil structure. It is important to note that one version of the peptide had the possibility of remaining completely random coil as it was bound to the AuNP through only a single linkage. This shows that the structural change in that peptide, and possibly both peptides, is primarily due to hydrophobic interactions between the peptide and the OEG monolayer. This finding is important because OEG layers are often used in conjunction with NPs to design NP−peptide conjugates.[7,57,58]

A second important point is that the AuNP−peptide conjugates presented here are soluble in water and have just three or four α-helix-structured peptides per AuNP. The combination of structure control and low peptide surface density creates an ideal model system for the tailored design of AuNP−peptide conjugates intended to show specific interactions with proteins. We are presently working to integrate these materials in technologically useful sensors.

MATERIALS AND METHODS

Chemicals and Materials. H_2SO_4, NaOH, NaCl, NH_4Cl, isopropanol, ethanol, toluene, and dichloromethane were purchased from Fisher Scientific (Waltham, MA, USA). $HAuCl_4{\cdot}3H_2O$, NaN_3, $NaBH_4$, anhydrous $MgSO_4$, tetraoctylammonium bromide, 4-(dimethylamino)pyridine, (11-mercaptoundecyl)tetra(ethylene glycol) (HS-C11-OEG4-OH), [11-(methylcarbonylthio)undecyl]tetra(ethylene glycol), triethylamine, sodium ascorbate, methyl sulfonyl chloride, acetyl chloride, *tert*-butyl alcohol (*t*-BuOH), methanol, and Amicon Ultra 0.5 mL 30 kDa molecular weight cutoff centrifugal filters were all purchased from Millipore Sigma (Burlington, MA, USA). Tris-hydroxypropyltriazolylmethylamine (THPTA) was purchased from Lumiprobe (Hunt Valley, MD, USA). $CuSO_4$(20% w/v) was purchased from Ricca Chemical Co. (Arlington, TX, USA). Synthetic peptides α-LK1X20 (H-LKKLXKKLLKKLLKKGLKKL-OH, X = propargylglycine), α-LK2X20 (H-LKKLXKKLLKKLLKKXLKKL-OH, X = propargylglycine), and α-LK2X20W (H-LKKLXKKLLKKLLKKXLKKLW-OH, X = propargylglycine) were purchased from WuXi AppTec (Shanghai, China). All aqueous solutions were prepared with DI water (>18.0 MΩ·cm, Milli-Q Gradient System, Millipore-Sigma, Burlington, MA, USA). [11-(Thio)undecyl]tetra(ethylene glycol)-azide (HS-C11-OEG4-N_3) was synthesized according to our previously published procedure.[17]

Synthesis and Characterization of AuNPs Capped with Azide and Hydroxyl-Terminated Alkylthiol/OEG Ligands (AuNP-OEG4-N_3/OH). AuNPs capped with HS-C11-OEG4-N_3 and HS-C11-OEG4-OH were synthesized according to a previously published procedure.[17,59] Briefly, an aqueous solution of $HAuCl_4$ (0.142 M, 0.700 mL) was added to a stirred mixture of tetraoctylammonium bromide in toluene (10.0 mL, 30.0 mM), and the resulting biphasic mixture was stirred vigorously for 30 min. Next, $NaBH_4$ (1.00 M, 1.00 mL) was added to the reaction mixture over the course of 1.0 s, and then the resulting AuNP mixture was stirred for 18 h at 21 °C. Next, the aqueous portion of the biphasic mixture was discarded, the toluene portion was washed with H_2SO_4 (0.100 M), NaOH (0.100 M), and DI water in succession, and this washing procedure was repeated three times. An aqueous solution of 4-(dimethylamino)pyridine (DMAP) (0.100 M, 10.0 mL) was added to the AuNP solution, and the resulting mixture was shaken vigorously for 3 min. It is important to note here that in our previously published procedure[17] the DMAP solution used in this step was indicated to be 10.0 mM. This was incorrect, and the actual concentration used previously and in the current work was 0.100 M. At this point, the wine-red color of the AuNPs shifted from the toluene phase to the aqueous phase. The toluene phase was discarded.

The resulting (DMAP)-capped AuNPs (10.0 mL, 2.49 μM) were added to an ethanolic solution (18.0 mL) containing HS-C11-OEG4-N_3 (1.36 mM) and HS-C11-OEG4-OH (4.09 mM). This mixture was incubated for 18 h at 21 °C, and then small molecule ligands not bound to AuNPs were removed from solution by filtration using Amicon Ultra, 30 kDa, 0.5 mL molecular weight cutoff (MWCO) filters. This purification consisted of loading the MWCO filter with 0.500 mL of AuNP solution followed by centrifugation at 14 000*g* for 10 min, and finally, 0.400 mL of 1:1 *t*-BuOH/water mixture was added to the retentate while the filtrate was discarded. This filtration and dilution procedure was repeated eight times.

Transmission electron microscopy (TEM, JEOL 2010 F) was used to determine the AuNP size distribution (4.6 ± 1.2 nm, Supporting Information, Figure S1).

Fourier transform infrared (FTIR) spectroscopy was used to characterize the ligand shell of the AuNPs (Figure S2). FTIR spectra were recorded using a Bruker Vertex 70 spectrometer equipped with a HgCdTe detector. To generate each FTIR spectrum, an AuNP solution (5.0 μL) was diluted into isopropanol (20.0 μL) and from this mixture 2.0 μL was drop cast onto each side of a CaF_2 window (random-angle cut, 2.0 mm width, 25.4 mm diameter). A total of 500 scans were averaged to generate blank and sample spectra (4 cm^{-1} resolution). The blank spectrum as well as a scaled spectrum of atmospheric water were subtracted from the sample spectrum. In addition, the spectral range between 2250 and 2400 cm^{-1} was set to baseline intensity to eliminate the CO_2 peak. Finally, baseline tilt in the sample spectrum was corrected using the OPUS Spectroscopic Software Straight Lines function (OPUS, 6.5.92, Bruker Optik, GmbH, Ettlingen, Germany). To account for differences in the number of AuNPs, the spectra of AuNPs were normalized to the height of the C−O stretching band at 1122 cm^{-1}.

The concentrations of the AuNP solutions were determined by UV−vis spectroscopy (Figure S4) and calculated from the molar extinction coefficient for 4.6 nm AuNPs reported by Huo and co-workers[60] ($\varepsilon_{506\ nm} = 8.56 \times 10^6$).

https://dx.doi.org/10.1021/acs.bioconjchem.0c00447
Bioconjugate Chem. 2020, 31, 2383−2391

Synthesis of AuNP−Peptide Conjugates. Alkyne-functionalized peptides were attached to AuNP-OEG4-N_3/OH using Cu^+-catalyzed azide−alkyne cycloaddition[38] as follows. A solution containing AuNP-OEG4-N_3/OH (0.0998 μM), sodium ascorbate (10.0 mM), $CuSO_4$ (10.0 μM), THPTA (20.0 μM), and α-LK2X20 or α-LK1X20 peptide (10.0 μM) (1:1 *t*-BuOH/water, 1.992 mL) was prepared (control solutions did not contain Cu^+). The solution was incubated overnight at 21 °C for 18 h. Next, the AuNPs were separated from unreacted peptide and other reagents by the filtration and washing protocol utilizing MWCO filters discussed in the previous section. Following this step, the solvent containing the AuNPs was exchanged for DI water by repeated filtration using MWCO filters (Amicon Ultra, 30 kDa, 0.5 mL) followed by addition of DI water (0.450 mL) to the AuNP solution. This solvent-exchange procedure was repeated a total of eight times. FTIR spectra of the AuNPs were recorded using the procedure described earlier (Figures 1 and S5).

The size distribution of AuNP-OEG4-N_3/OH-α-LK1X20 was 4.5 ± 1.1 nm (TEM, Supporting Information, Figure S9), and for AuNP-OEG4-N_3/OH-α-LK2X20 it was 4.4 ± 0.9 nm (TEM, Supporting Information, Figure S10).

Circular Dichroism Spectroscopy. CD spectra of the materials discussed in this work (Figures 2, S7, and S8) were obtained using a JASCO J-815 CD spectrometer. A quartz cuvette (1.00 mm path length) was used in all cases. Spectra were recorded from 250 to 190 nm, the bandwidth was set to 1 nm, the response time was 4 s, and the scan rate was 50 nm/min. For all AuNP-containing samples, a blank spectrum of DI water was obtained from 300 averaged scans, and a sample spectrum was obtained using 500 averaged scans. The blank spectrum was then subtracted from the sample spectrum. For samples containing only peptides, blank and sample spectra were obtained from six averaged scans and the blank spectrum was subtracted from the sample spectrum. Finally, the CD signal intensity at 250 nm was subtracted from all spectra (Spectra Manager for Windows, 1.24.00, JASCO Corp., Tokyo, Japan).

Amino acid analysis testing of the AuNP−peptide conjugates was performed by the Protein Chemistry Laboratory at Texas A&M University (College Station, TX, USA)

■ ASSOCIATED CONTENT

Supporting Information

The Supporting Information is available free of charge at https://pubs.acs.org/doi/10.1021/acs.bioconjchem.0c00447.

TEM analysis of AuNP-OEG4-N_3/OH; FTIR spectrum of AuNP-OEG4-N_3/OH; description of the FTIR spectrum of AuNP-OEG4-N_3/OH; FTIR spectra of AuNP-OEG4-N_3/OH and AuNP-OEG4-N_3; calculation of the percentage of azide groups in the ligand shell of AuNP-OEG4-N_3/OH; UV−vis spectra of AuNPs; FTIR spectra of α-LK2X20, AuNP-OEG4-N_3/OH-α-LK2X20, and AuNP-OEG4-N_3/OH incubated with α-LK2X20 but not Cu^+ and then filtered from unreacted peptide; calibration curve of amino acid analysis-reported concentration of α-LK2X20W peptide in solutions of known peptide concentration; details of the amino acid analysis control experiments; CD spectrum of AuNP-OEG4-N_3/OH with no attached peptide; raw and unmodified CD spectra of AuNP-OEG4-N_3/OH-α-LK1X20 and the corresponding solvent blank spectrum of DI water; TEM analysis of AuNP-OEG4-N_3/OH-α-LK1X20; TEM analysis of AuNP-OEG4-N_3/OH-α-LK2X20; ligand length of AuNP-OEG4-N_3/OH; CD background subtraction method; normalized FTIR absorption intensity of the azide peak at 2101 cm^{-1} of AuNP materials; calculation of the number of azide groups per AuNP (PDF)

■ AUTHOR INFORMATION

Corresponding Authors

Lauren J. Webb − *Department of Chemistry and Texas Materials Institute, The University of Texas at Austin, Austin, Texas 78712-1224, United States;* orcid.org/0000-0001-9999-5500; Email: lwebb@cm.utexas.edu

Richard M. Crooks − *Department of Chemistry and Texas Materials Institute, The University of Texas at Austin, Austin, Texas 78712-1224, United States;* orcid.org/0000-0001-5186-4878; Email: crooks@cm.utexas.edu

Authors

Logan M. Wilder − *Department of Chemistry and Texas Materials Institute, The University of Texas at Austin, Austin, Texas 78712-1224, United States*

Paul R. Handali − *Department of Chemistry and Texas Materials Institute, The University of Texas at Austin, Austin, Texas 78712-1224, United States*

Complete contact information is available at: https://pubs.acs.org/10.1021/acs.bioconjchem.0c00447

Notes

The authors declare no competing financial interest.

■ ACKNOWLEDGMENTS

This work was supported by the U.S. Army Research Office under Grant No. W911NF-17-1-0089. We also thank the Robert A. Welch Foundation for sustained support of our research (R.M.C., Grant No. F-0032; L.J.W., Grant No. F-1722). We thank Dr. Jeremy T. First for helpful advice on the application of BeStSel CD deconvolution to surface-bound peptide CD spectra. We also thank the Texas A&M Protein Chemistry Laboratory for amino acid analysis of peptide samples. We gratefully acknowledge use of the facilities of the UT—Austin Targeted Therapeutic Drug Discovery & Development Program and the facilities of the UT—Austin Texas Materials Institute.

■ ABBREVIATIONS

NP, nanoparticle; OEG, oligoethylene glycol; EG, ethylene glycol, PEG, polyethylene glycol; Aβ, amyloid-beta peptide; FTIR, Fourier transform infrared; CD, circular dichroism; AAA, amino acid analysis; HS-C11-OEG4-OH, HS-$(CH_2)_{11}$-O-$(CH_2$-CH_2-$O)_3$-CH_2-CH_2-OH; HS-C11-OEG4-N_3, HS-$(CH_2)_{11}$-O-$(CH_2$-CH_2-$O)_3$-CH_2-CH_2-N_3; α-LK1X20, H-LKKLXKKLLKKLLKKGLKKL-OH, where X = propargylglycine; α-LK2X20, H-LKKLXKKLLKKLLKKXLKKL-OH, where X = propargylglycine; α-LK2X20W, H-LKKLXKKLLKKLLKKXLKKLW-OH, where X = propargylglycine; CuAAC, Cu^+-catalyzed azide−alkyne cycloaddition; TEM, transmission electron microscopy; DI, deionized; NRMSD, normalized root-mean-square deviation; *t*-BuOH,

https://dx.doi.org/10.1021/acs.bioconjchem.0c00447
Bioconjugate Chem. 2020, 31, 2383−2391

tert-butyl alcohol; THPTA, tris-hydroxypropyltriazolylmethylamine; DMAP, 4-(dimethylamino)pyridine; MWCO, molecular weight cutoff

REFERENCES

(1) Jeong, W.-J., Bu, J., Kubiatowicz, L. J., Chen, S. S., Kim, Y. S., and Hong, S. (2018) Peptide-Nanoparticle Conjugates: A next Generation of Diagnostic and Therapeutic Platforms? *Nano Convergence 5*, 1−18.

(2) Kogan, M. J., Olmedo, I., Hosta, L., Guerrero, A. R., Cruz, L. J., and Albericio, F. (2007) Peptides and Metallic Nanoparticles for Biomedical Applications. *Nanomedicine 2*, 287−306.

(3) Spicer, C. D., Jumeaux, C., Gupta, B., and Stevens, M. M. (2018) Peptide and Protein Nanoparticle Conjugates: Versatile Platforms for Biomedical Applications. *Chem. Soc. Rev. 47*, 3574−3620.

(4) Barua, S., and Mitragotri, S. (2014) Challenges Associated with Penetration of Nanoparticles across Cell and Tissue Barriers: A Review of Current Status and Future Prospects. *Nano Today 9*, 223−243.

(5) Blanco-Canosa, J. B., Wu, M., Susumu, K., Petryayeva, E., Jennings, T. L., Dawson, P. E., Algar, W. R., and Medintz, I. L. (2014) Recent Progress in the Bioconjugation of Quantum Dots. *Coord. Chem. Rev. 263−264*, 101−137.

(6) Olmedo, I., Araya, E., Sanz, F., Medina, E., Arbiol, J., Toledo, P., Álvarez-Lueje, A., Giralt, E., and Kogan, M. J. (2008) How Changes in the Sequence of the Peptide CLPFFD-NH_2 Can Modify the Conjugation and Stability of Gold Nanoparticles and Their Affinity for β-Amyloid Fibrils. *Bioconjugate Chem. 19*, 1154−1163.

(7) Kim, B., Choi, S.-J., Han, S.-H., Choi, K.-Y., and Lim, Y.-B. (2013) Stabilization of α-Helices by the Self-Assembly of Macrocyclic Peptides on the Surface of Gold Nanoparticles for Molecular Recognition. *Chem. Commun. 49*, 7617−7619.

(8) Read, M. J., and Burkett, S. L. (2003) Asymmetric α-Helicity Loss within a Peptide Adsorbed onto Charged Colloidal Substrates. *J. Colloid Interface Sci. 261*, 255−263.

(9) Mandal, H. S., and Kraatz, H.-B. (2007) Effect of the Surface Curvature on the Secondary Structure of Peptides Adsorbed on Nanoparticles. *J. Am. Chem. Soc. 129*, 6356−6357.

(10) Slocik, J. M., and Naik, R. R. (2010) Probing Peptide-Nanomaterial Interactions. *Chem. Soc. Rev. 39*, 3454−3463.

(11) Checco, J. W., and Gellman, S. H. (2016) Targeting Recognition Surfaces on Natural Proteins with Peptidic Foldamers. *Curr. Opin. Struct. Biol. 39*, 96−105.

(12) Pengo, P., Broxterman, Q. B., Kaptein, B., Pasquato, L., and Scrimin, P. (2003) Synthesis of a Stable Helical Peptide and Grafting on Gold Nanoparticles. *Langmuir 19*, 2521−2524.

(13) Higashi, N., Kawahara, J., and Niwa, M. (2005) Preparation of Helical Peptide Monolayer-Coated Gold Nanoparticles. *J. Colloid Interface Sci. 288*, 83−87.

(14) Fabris, L., Antonello, S., Armelao, L., Donkers, R. L., Polo, F., Toniolo, C., and Maran, F. (2006) Gold Nanoclusters Protected by Conformationally Constrained Peptides. *J. Am. Chem. Soc. 128*, 326−336.

(15) Nygren, P., Lundqvist, M., Broo, K., and Jonsson, B.-H. (2008) Fundamental Design Principles That Guide Induction of Helix upon Formation of Stable Peptide-Nanoparticle Complexes. *Nano Lett. 8*, 1844−1852.

(16) Verma, A., Nakade, H., Simard, J. M., and Rotello, V. M. (2004) Recognition and Stabilization of Peptide α-Helices Using Templatable Nanoparticle Receptors. *J. Am. Chem. Soc. 126*, 10806−10807.

(17) Wilder, L. M., Fies, W. A., Rabin, C., Webb, L. J., and Crooks, R. M. (2019) Conjugation of an α-Helical Peptide to the Surface of Gold Nanoparticles. *Langmuir 35*, 3363−3371.

(18) Lau, Y. H., de Andrade, P., Wu, Y., and Spring, D. R. (2015) Peptide Stapling Techniques Based on Different Macrocyclisation Chemistries. *Chem. Soc. Rev. 44*, 91−102.

(19) Pelaz, B., del Pino, P., Maffre, P., Hartmann, R., Gallego, M., Rivera-Fernández, S., de la Fuente, J. M., Nienhaus, G. U., and Parak, W. J. (2015) Surface Functionalization of Nanoparticles with Polyethylene Glycol: Effects on Protein Adsorption and Cellular Uptake. *ACS Nano 9*, 6996−7008.

(20) Love, J. C., Estroff, L. A., Kriebel, J. K., Nuzzo, R. G., and Whitesides, G. M. (2005) Self-Assembled Monolayers of Thiolates on Metals as a Form of Nanotechnology. *Chem. Rev. 105*, 1103−1169.

(21) Sapsford, K. E., Algar, W. R., Berti, L., Gemmill, K. B., Casey, B. J., Oh, E., Stewart, M. H., and Medintz, I. L. (2013) Functionalizing Nanoparticles with Biological Molecules: Developing Chemistries That Facilitate Nanotechnology. *Chem. Rev. 113*, 1904−2074.

(22) Hermanson, G. T. (2013) Microparticles and Nanoparticles. *Bioconjugate Techniques*, 3rd ed. (Audet, J., and Preap, M., Eds.) pp 549−587, Chapter 14, Elsevier, Amsterdam.

(23) Sivaram, A. J., Wardiana, A., Howard, C. B., Mahler, S. M., and Thurecht, K. J. (2018) Recent Advances in the Generation of Antibody-Nanomaterial Conjugates. *Adv. Healthcare Mater. 7*, 1700607.

(24) Brennan, J. L., Hatzakis, N. S., Tshikhudo, T. R., Dirvianskyte, N., Razumas, V., Patkar, S., Vind, J., Svendsen, A., Nolte, R. J. M., Rowan, A. E., et al. (2006) Bionanoconjugation via Click Chemistry: The Creation of Functional Hybrids of Lipases and Gold Nanoparticles. *Bioconjugate Chem. 17*, 1373−1375.

(25) Moyano, D. F., and Rotello, V. M. (2011) Nano Meets Biology: Structure and Function at the Nanoparticle Interface. *Langmuir 27*, 10376−10385.

(26) Brambilla, D., Verpillot, R., Le Droumaguet, B., Nicolas, J., Taverna, M., Kóňa, J., Lettiero, B., Hashemi, S. H., De Kimpe, L., Canovi, M., et al. (2012) PEGylated Nanoparticles Bind to and Alter Amyloid-Beta Peptide Conformation: Toward Engineering of Functional Nanomedicines for Alzheimer's Disease. *ACS Nano 6*, 5897−5908.

(27) Liu, Y., Shipton, M. K., Ryan, J., Kaufman, E. D., Franzen, S., and Feldheim, D. L. (2007) Synthesis, Stability, and Cellular Internalization of Gold Nanoparticles Containing Mixed Peptide-Poly(Ethylene Glycol) Monolayers. *Anal. Chem. 79*, 2221−2229.

(28) Link, S., and El-Sayed, M. A. (1999) Size and Temperature Dependence of the Plasmon Absorption of Colloidal Gold Nanoparticles. *J. Phys. Chem. B 103*, 4212−4217.

(29) Harder, P., Grunze, M., Dahint, R., Whitesides, G. M., and Laibinis, P. E. (1998) Molecular Conformation in Oligo(Ethylene Glycol)-Terminated Self-Assembled Monolayers on Gold and Silver Surfaces Determines Their Ability To Resist Protein Adsorption. *J. Phys. Chem. B 102*, 426−436.

(30) Mayer, K. M., and Hafner, J. H. (2011) Localized Surface Plasmon Resonance Sensors. *Chem. Rev. 111*, 3828−3857.

(31) Weidner, T., Breen, N. F., Li, K., Drobny, G. P., and Castner, D. G. (2010) Sum Frequency Generation and Solid-State NMR Study of the Structure, Orientation, and Dynamics of Polystyrene-Adsorbed Peptides. *Proc. Natl. Acad. Sci. U. S. A. 107*, 13288−13293.

(32) Collier, G., Vellore, N. A., Yancey, J. A., Stuart, S. J., and Latour, R. A. (2012) Comparison between Empirical Protein Force Fields for the Simulation of the Adsorption Behavior of Structured LK Peptides on Functionalized Surfaces. *Biointerphases 7*, 24.

(33) Long, J. R., Oyler, N., Drobny, G. P., and Stayton, P. S. (2002) Assembly of α-Helical Peptide Coatings on Hydrophobic Surfaces. *J. Am. Chem. Soc. 124*, 6297−6303.

(34) Deighan, M., and Pfaendtner, J. (2013) Exhaustively Sampling Peptide Adsorption with Metadynamics. *Langmuir 29*, 7999−8009.

(35) Baio, J. E., Zane, A., Jaeger, V., Roehrich, A. M., Lutz, H., Pfaendtner, J., Drobny, G. P., and Weidner, T. (2014) Diatom Mimics: Directing the Formation of Biosilica Nanoparticles by Controlled Folding of Lysine-Leucine Peptides. *J. Am. Chem. Soc. 136*, 15134−15137.

(36) Apte, J. S., Collier, G., Latour, R. A., Gamble, L. J., and Castner, D. G. (2010) XPS and ToF-SIMS Investigation of α-Helical and β-Strand Peptide Adsorption onto SAMs. *Langmuir 26*, 3423−3432.

(37) Mermut, O., Phillips, D. C., York, R. L., McCrea, K. R., Ward, R. S., and Somorjai, G. A. (2006) In Situ Adsorption Studies of a 14-Amino Acid Leucine-Lysine Peptide onto Hydrophobic Polystyrene

https://dx.doi.org/10.1021/acs.bioconjchem.0c00447
Bioconjugate Chem. 2020, 31, 2383−2391

and Hydrophilic Silica Surfaces Using Quartz Crystal Microbalance, Atomic Force Microscopy, and Sum Frequency Generation Vibrational Spectroscopy. *J. Am. Chem. Soc. 128*, 3598−3607.
(38) Meldal, M., and Tornøe, C. W. (2008) Cu-Catalyzed Azide-Alkyne Cycloaddition. *Chem. Rev. 108*, 2952−3015.
(39) Hinterwirth, H., Kappel, S., Waitz, T., Prohaska, T., Lindner, W., and Lämmerhofer, M. (2013) Quantifying Thiol Ligand Density of Self-Assembled Monolayers on Gold Nanoparticles by Inductively Coupled Plasma-Mass Spectrometry. *ACS Nano 7*, 1129−1136.
(40) Fountoulakis, M., and Lahm, H.-W. (1998) Hydrolysis and Amino Acid Composition Analysis of Proteins. *J. Chromatogr. A 826*, 109−134.
(41) DeGrado, W. F., and Lear, J. D. (1985) Induction of Peptide Conformation at Apolar/Water Interfaces. 1. A Study with Model Peptides of Defined Hydrophobic Periodicity. *J. Am. Chem. Soc. 107*, 7684−7689.
(42) Dugger, J. W., and Webb, L. J. (2015) Preparation and Characterization of Biofunctionalized Inorganic Substrates. *Langmuir 31*, 10331−10340.
(43) Wiradharma, N., Khan, M., Yong, L.-K., Hauser, C. A. E., Seow, S. V., Zhang, S., and Yang, Y.-Y. (2011) The Effect of Thiol Functional Group Incorporation into Cationic Helical Peptides on Antimicrobial Activities and Spectra. *Biomaterials 32*, 9100−9108.
(44) Blondelle, S. E., and Houghten, R. A. (1992) Design of Model Amphipathic Peptides Having Potent Antimicrobial Activities. *Biochemistry 31*, 12688−12694.
(45) Gallardo, I. F., and Webb, L. J. (2012) Demonstration of α-Helical Structure of Peptides Tethered to Gold Surfaces Using Surface Infrared and Circular Dichroic Spectroscopies. *Langmuir 28*, 3510−3515.
(46) White, S. J., Johnson, S. D., Sellick, M. A., Bronowska, A., Stockley, P. G., and Wälti, C. (2015) The Influence of Two-Dimensional Organization on Peptide Conformation. *Angew. Chem., Int. Ed. 54*, 974−978.
(47) Johnson, W. C. (1988) Secondary Structure of Proteins Through Circular Dichroism Spectroscopy. *Annu. Rev. Biophys. Biophys. Chem. 17*, 145−166.
(48) Wei, Y., Thyparambil, A. A., and Latour, R. A. (2014) Protein Helical Structure Determination Using CD Spectroscopy for Solutions with Strong Background Absorbance from 190 to 230 nm. *Biochim. Biophys. Acta, Proteins Proteomics 1844*, 2331−2337.
(49) Micsonai, A., Wien, F., Bulyáki, É., Kun, J., Moussong, É., Lee, Y.-H., Goto, Y., Réfrégiers, M., and Kardos, J. (2018) BeStSel: A Web Server for Accurate Protein Secondary Structure Prediction and Fold Recognition from the Circular Dichroism Spectra. *Nucleic Acids Res. 46*, W315−W322.
(50) Micsonai, A., Wien, F., Kernya, L., Lee, Y.-H., Goto, Y., Réfrégiers, M., and Kardos, J. (2015) Accurate Secondary Structure Prediction and Fold Recognition for Circular Dichroism Spectroscopy. *Proc. Natl. Acad. Sci. U. S. A. 112*, E3095−E3103.
(51) Greenfield, N. J. (1996) Methods to Estimate the Conformation of Proteins and Polypeptides from Circular Dichroism Data. *Anal. Biochem. 235*, 1−10.
(52) Shemetov, A. A., Nabiev, I., and Sukhanova, A. (2012) Molecular Interaction of Proteins and Peptides with Nanoparticles. *ACS Nano 6*, 4585−4602.
(53) Hall, T. M. T. (2005) Multiple Modes of RNA Recognition by Zinc Finger Proteins. *Curr. Opin. Struct. Biol. 15*, 367−373.
(54) Battiste, J. L., Mao, H., Rao, N. S., Tan, R., Muhandiram, D. R., Kay, L. E., Frankel, A. D., and Williamson, J. R. (1996) α-Helix-RNA Major Groove Recognition in an HIV-1 Rev Peptide-RRE RNA Complex. *Science 273*, 1547−1551.
(55) Kussie, P. H., Gorina, S., Marechal, V., Elenbaas, B., Moreau, J., Levine, A. J., and Pavletich, N. P. (1996) Structure of the MDM2 Oncoprotein Bound to the p53 Tumor Suppressor Transactivation Domain. *Science 274*, 948−953.
(56) Dash, S., Niemaczura, W., and Harrington, H. M. (1997) Characterization of the Basic Amphiphilic α-Helix Calmodulin-Binding Domain of a 61.5 KDa Tobacco Calmodulin-Binding Protein. *Biochemistry 36*, 2025−2029.
(57) Harrison, E., Nicol, J. R., Macias-Montero, M., Burke, G. A., Coulter, J. A., Meenan, B. J., and Dixon, D. (2016) A Comparison of Gold Nanoparticle Surface Co-Functionalization Approaches Using Polyethylene Glycol (PEG) and the Effect on Stability, Non-Specific Protein Adsorption and Internalization. *Mater. Sci. Eng., C 62*, 710−718.
(58) Krpetić, Ž., Saleemi, S., Prior, I. A., Sée, V., Qureshi, R., and Brust, M. (2011) Negotiation of Intracellular Membrane Barriers by TAT-Modified Gold Nanoparticles. *ACS Nano 5*, 5195−5201.
(59) Gittins, D. I., and Caruso, F. (2001) Spontaneous Phase Transfer of Nanoparticulate Metals from Organic to Aqueous Media. *Angew. Chem., Int. Ed. 40*, 3001−3004.
(60) Liu, X., Atwater, M., Wang, J., and Huo, Q. (2007) Extinction Coefficient of Gold Nanoparticles with Different Sizes and Different Capping Ligands. *Colloids Surf., B 58*, 3−7.

https://dx.doi.org/10.1021/acs.bioconjchem.0c00447
Bioconjugate Chem. 2020, 31, 2383−2391